Heliyon 7 (2021) e06338

Contents lists available at ScienceDirect

Heliyon

journal homepage: www.cell.com/heliyon

Research article

Surface roughness prediction using a hybrid scheme of difference analysis and adaptive feedback weights

M.K.O. Ayomoh [a,*], K.A. Abou-El-Hossein [b]

[a] Industrial and Systems Engineering Department, University of Pretoria, 0028, Hatfield, South Africa
[b] Mechatronics Engineering Department, Nelson Mandela University, North Campus, Summerstrand, 6001, Port Elizabeth, South Africa

ARTICLE INFO

Keywords:
Adaptive weights
On-edge cutting combinations
Off-edge cutting combinations
Difference analysis
Surface roughness prediction
Feedback control

ABSTRACT

This research has presented an optimum model for surface roughness prediction in a shop floor machining operation. The proposed solution is premised on difference analysis enhanced with a feedback control model capable of generating transient adaptive weights until a converging set point is attained. The surface roughness results utilized herein were adopted from two prior experiments in the literature. The design of experiment herein is premised on three cutting parameters in both experimental scenarios viz: feed rate, cutting speed and depth of cut for experimental dataset one and cutting speed, feed rate and flow rate for experimental dataset two. Three experimental levels were considered in both scenarios resulting in twenty-seven outcomes each. The simulation trial anchored on Matlab software was divided into two sub-categories viz: prediction of surface roughness for cutting combinations with vector points off the edges of the mesh referred to as off-edge cutting combinations (Off-ECC) and recovery of cutting combinations with positions on the edges of the mesh referred to as on-edge cutting combinations (On-ECC). The proposed hybrid scheme of difference analysis with feedback control premised on the use of dynamic weights produced an accurate output in comparison with the abductive, regression analysis and artificial neural network techniques as earlier utilized in the literature. The novelty of the proposed hybrid model lies in its high degree of prediction and recovery of existing datasets with an error margin approximately zero. This predictive efficacy is premised on the use of set points and transient dynamic weights for feedback iterations. The proposed solution technique in this research is quite consistent with its outputs and capable of working with very small to complex datasets.

1. Introduction

Predictive analysis of inherent dynamic behaviours associated with some properties of engineering materials over a given time horizon is of a significant research interest in the literature. Quite a number of economic benefits are accruable to effectiveness in predictive modelling of systems outputs ranging from minimization of the overall operational cost bothering around experimental set-up time to the cost of human resources, material resources utilization and other miscellaneous financial implications. A recent trend across production systems globally is the need to introduce and implement functional lean driven mechanisms Greinacher et al. (2020) to predict dynamic effects ranging from materials through energy and information flow amongst others. The effectiveness in predicting dynamic behaviour of systems is a key driver of lean based operations capable of reducing wastes and overall operational cost. Machining is a vital engineering operation across the globe that seeks to attain a zero error margin between the predicted and experimental datasets especially in mission critical systems and artificial intelligence based systems Weichert et al. (2019) with a high degree of intolerance for measurement discrepancy. Predictive modelling of surface finish premised on the interactions between mathematical models and machining parameters is about the most objective approach for roughness estimation and can be referred to as next-to-experimentation. Amongst the diverse properties of materials considered in surface worthiness assessment, roughness is considered to be of a very high esteem from modern day computer chips manufacturing to other mission critical products utilised in the aerospace and medical industry amongst others. Roughness under any form of inspection or observatory measure is a function of the physical appearance of a given engineering material. More often than not, this property cannot be accurately inferred using mere human sensations or visual inspection. Quite a number of techniques have been utilized over the years to carry out roughness

* Corresponding author.
E-mail address: michael.ayomoh@up.ac.za (M.K.O. Ayomoh).

https://doi.org/10.1016/j.heliyon.2021.e06338
Received 1 June 2019; Received in revised form 3 July 2019; Accepted 18 February 2021

measurement of machined surfaces. These techniques Zhao and Gao (2009) spread across the use of subjective judgemental schemes based on human visual inspection premised on the sense of sight to the fingernail test based on the sense of touch amongst others. Some notable objective techniques utilized over the years include: ultrasound, pneumatics, inductance and capacitance methods, the contact mechanical stylus device to the low-powered optical microscope, non-contact optical profilers, the more recent scanning-tunnelling microscope (STM) and the atomic force microscopy (AFM) amongst others. This paper has presented a novel predictive solution premised on a developed numerical solution using Gauss-Seidel's technique coupled with a developed adaptive weight feedback scheme using set points. The proposed solution was validated using experimental data from the literature Lin et al. (2001) and Mia et al. (2017). The primary goal of this research is to apply the developed predictive model to selected experimental datasets and generate both numerical and graphical outputs to serve as a basis for objective comparison of the degree of efficacy of the proposed technique and selected existing techniques from the literature.

Ayomoh et al. (2015) proposed a hybrid scheme of difference analysis and dynamic weights anchored on a feedback concept for prediction of surface roughness of machined surfaces. Feng et al. (2012) undertook a study focused at measuring both RMS and Ra readings for a cast alloy substrate with alumina buffered layer surfaces while Bajić et al. (2012) deployed a combination of regression analysis and neural network solution for examination of cutting force, surface roughness and tool wear during a milling operation. An artificial neural network based technique was proposed by Rao et al. (2014) for surface coarseness prediction of stainless steel while a geometrical based modelling approach was applied by Munoz-Escalona and Maropoulos (2015) for surface roughness prediction while face milling with square inserts. Burakowski et al. (2018), evaluated the bio-physical factors which contributes to local surface temperature disparity. The remarks and modelling procedure suggested that the coarseness attributes contributed significantly to the local temperature disparity. In their work, Yang et al. (2018) investigated how surface roughness influences contact line dynamics by simulating forced wetting in a capillary tube. Asiltürk et al. (2016) developed and proposed a set of mathematical models to determine multi-objective optimal cutting conditions. Debnath et al. (2016) worked on the combined influence of fluid condition and cutting parameters on surface coarseness and tool-life. They also looked at optimizing cutting parameters in order to attain a good surface roughness and prolonged tool life. Zhang and Shetty (2016) proposed a least square support vector machine for the prediction of surface roughness in machined surfaces. Tangjitsitcharoen et al. (2017) proposed an approach for the prediction of an in-process surface roughness measurement in a ball end milling task via utilization of a non-static cutting force ratio.

In their study, Taufik and Jain (2016) proposed a scheme by combining both theoretical and pragmatic approaches for the analysis and prediction of randomness in the shape of built-edge profiles. Vahabli and Rahmati (2016), proposed an approach premised on radial basis function neural networks (RBFNNs) for computation of surface roughness readings in relation to that obtained from experimentations. Ding et al. (2010) carried out an experimental research on investigation of the effects of cutting parameters on surface roughness and cutting force. A comparative study was carried out by Lee et al. (2010) on surface roughness using the Atomic Force Microscope (AFM) while a combination of experimentations and analysis were carried out by Xie et al. (2011) on crack formation using AFM and Scanning Electron Microscope (SEM). Karkalos et al. (2016) investigated the effects of machining process parameters on roughness while conducting a milling operation of Ti–6Al–4V ELI titanium alloy. Khorasani and Yazdi (2017) proposed a dynamic surface coarseness monitoring system for a milling operation while Bao et al. (2018) addressed the influence of operational parameters on surface roughness using the interactions between normal pressure and surface roughness. The response surface method (RSM) was utilised in the development of a predictive model for surface coarseness in micro-milling operation of Inconel 718 Lu et al. (2018) while Plaza and López (2018) worked on techniques for processing cutting force signals based on the wavelet packet transform (WPT) method for the monitoring of surface finish in computer numerical control (CNC) turning operations. Hussain et al. (2018) investigated the performance of a newly designed lapping tool in terms of surface roughness. Their study showed that polypropylene is able to produce good quality and smooth surface roughness. Gopal and Prakash (2018) investigated the effect of material and machining parameters on cutting force, surface roughness and temperature in end milling of Magnesium Metal Matrix Composite (MMC) using carbide tool.

Balaji et al. (2018) studied the effect of drilling parameters such as spindle speed, helix angle and feed rate on surface roughness, flank wear and acceleration of drill vibration velocity using Response Surface Methodology. Romoli (2018) carried out Micro-milling of AISI 316L using a scanning strategy based on spiral trajectories. The aim is twofold: i.e. reducing the surface roughness and ensuring a uniform depth of cut per layer. Ali et al. (2018) carried out a study to discover the effect of cutting speed and feed rate on the performance of the ZTA-MgO cutting tool via wear and surface roughness measurement. Pashmforoush and Bagherinia (2018) studied the effect of using environmentally friendly water-based copper nano-fluid in grinding performance of Inconel 738 super alloy. The results obtained revealed that application of copper nanofluid could improve wheel loading and surface roughness. Ünal (2018) studied the Influence of drilling parameters on temperature and surface roughness of AISI O2 steel. Natasha et al. (2018) investigated the effects of machining conditions such as: dry and cryogenic and also the machining tool wear on the surface roughness of AISI 4340 steel. Experimental tests were performed using chemical vapour deposition (CVD) coated carbide inserts. Ahmed et al. (2018) carried out some electrical discharge machining process which serves as a material removal process especially in machining of difficult metals with high electrical conductivity. Scifo et al. (2018) worked on Cu photocathodes in a nano-machining process. This procedure according to them can reduce the coarseness of the cathode surface hence preventing the contamination of surfaces based on other techniques. Lin et al. (2018) presented experimentations in relation to the variation of quality factor of WGM resonators as a function of surface roughness.

Girinon et al. (2019) worked on drilling process control for surface integrity of metallic components with an austenitic stainless steel 316L used as a case study. Bahgat et al. (2019; 2020) applied a non-traditional machining process namely the electrical discharge machining (EDM) process used for machining of hard materials and to produce complicated shapes. They investigated different electrical discharge machining (EDM) process parameters on H13 die steel and alloyed tool steel respectively. Some parameters considered in their experiment include peak current (I_p), pulse on-time (T_{on}), electrode material and polarity. The Taguchi method was used to investigate the significant effect of process parameters on the performance measurements and the optimal parameters of the EDM process. The machining process was evaluated by the material removal rate (MRR), electrode wear ratio (EW%), and surface roughness (SR) as indicators of the process efficiency in terms of quality and cost. Chen and Ho (2019) conducted a research that mainly used Waspaloy of nickel base material for a cutting process. They further utilised regression analysis to find significant factor of the cutting tool's life and performed an optimization experiment. Dumitru and Maria (2013) discussed the merits and demerits of ANN systems. According to their research work, ANN has the ability to learn and model nonlinear and complex relationships however, its black box nature i.e. inability to explain why a decision was taken, greater computational burden, proneness to overfitting amongst others can be a big challenge. Furthermore, they stated that ANN models are universal approximators hence, they work best if the system being modelled has a high tolerance for error.

2. Experimental procedure

This section presents some details on the experimental procedure, set-up schematic and design of experiment as adapted from Lin et al. (2001) and Mia et al. (2017). The sketched experimental set-up in Figure 1 was carried out using S55C high-carbon-steel on a lathe machine with a sintered carbide insertion aimed at measuring the surface roughness with the aid of a surface-tester and Surfcorder SE-3030H. The cutting parameters and experimental levels are as presented in Tables 1 and 2. Three factors and levels are contained in Table 1 while Table 2 presents 27 experimental cutting combinations based on the design of experiment.

The time-controlled experimental set-up in Figure 2, Mia et al. (2017) utilised a cutting tool made up of an uncoated cemented carbide insert (SNMM 120408) placed on PSBNR 2525M12 tool holder. The experiment which focused on the turning of hardened steel in a centre lathe, allowed for a maximum work piece length of 1m. The cutting parameters, experimental levels and sample space are as presented in Tables 3 and 4. Three factors and levels are presented in Table 1 while Table 2 contains twenty-seven experimental cutting combinations based on the experimental design.

3. Modelling

3.1. Difference analysis

The predictive model presented in this paper was developed using a 3-Dimension Gauss-Seidel diagonal and standard five point techniques. With respect to Table 2, the experimental factors viz: depth of cut, feed rate and cutting speed were denoted with the modelling notationswhile same modelling notations were used to denote experimental factors: depth of cut, feed rate and flow rate in Table 4. These, represents the various cutting combinations used as the surface roughness predictive function (u) given as: . Upon considering the difference analysis along the (*a*,*b and c*) coordinates, Eqs. (1), (2), (3), (4), (5), and (6) was developed. Consideration of the a-axis, resulted in models (1) and (2):

$$g(a+\alpha,b,c)=g(a,b,c)+\alpha\frac{\partial u}{\partial a}+\frac{1}{2!}\alpha^2\frac{\partial^2 u}{\partial a^2}+\frac{1}{3!}+\alpha^3\frac{\partial^3 u}{\partial a^3}+\ldots\ldots \tag{1}$$

and

$$g(a-\alpha,b,c)=g(a,b,c)-\alpha\frac{\partial u}{\partial a}+\frac{1}{2!}\alpha^2\frac{\partial^2 u}{\partial a^2}-\frac{1}{3!}\alpha^3\frac{\partial^3 u}{\partial a^3}+\ldots\ldots \tag{2}$$

For b-axis, the following models (3) and (4) representing the forward and backward difference model were developed:

$$g(a,b+\beta,c)=g(a,b,c)+\beta\frac{\partial u}{\partial b}+\frac{1}{2!}\beta^2\frac{\partial^2 u}{\partial b^2}+\frac{1}{3!}\beta^3\frac{\partial^3 u}{\partial b^3}+\ldots\ldots \tag{3}$$

and

$$g(a,b-\beta,c)=g(a,b,c)-\beta\frac{\partial u}{\partial b}+\frac{1}{2!}\beta^2\frac{\partial^2 u}{\partial b^2}-\frac{1}{3!}\beta^3\frac{\partial^3 u}{\partial b^3}+\ldots\ldots \tag{4}$$

considering the c axis results in:

$$g(a,b,c+\gamma)=g(a,b,c)+\gamma\frac{\partial u}{\partial c}+\frac{1}{2!}\gamma^2\frac{\partial^2 u}{\partial c^2}+\frac{1}{3!}\gamma^3\frac{\partial^3 u}{\partial c^3}+\ldots\ldots \tag{5}$$

and

$$g(a,b,c-\gamma)=g(a,b,c)-\gamma\frac{\partial u}{\partial c}+\frac{1}{2!}\gamma^2\frac{\partial^2 u}{\partial c^2}-\frac{1}{3!}\gamma^3\frac{\partial^3 u}{\partial c^3}+\ldots\ldots \tag{6}$$

Eliminating, and higher powers of , and from all of Eqs. (1), (2), (3), (4), (5), and (6) followed by subtraction of Eq. (2) from (1), Eq. (4) from (3) and Eq. (6) from (5) resulted in the central difference model. On adding Eqs. (1) and (2), Eqs. (3) and (4) and Eqs. (5) and (6) and eliminating, and higher powers of , andresulted in the Laplace's equation as presented in (7).

$$\frac{\partial^2 u}{\partial a^2}+\frac{\partial^2 u}{\partial b^2}+\frac{\partial^2 u}{\partial c^2}=0 \tag{7}$$

Given that represents a unit increase along the axes a, b and c respectively, Eq. (7) can be re-written as:

$$g(a,b,c)=\frac{1}{6}[g(a+\alpha,b,c)+g(a-\alpha,b,c)+g(a,b+\beta,c)+g(a,b-\beta,c)+g(a,b,c+\gamma)+g(a,b,c-\gamma)] \tag{8}$$

$$g_{i,j,k}=\frac{\varpi_i}{6}\left[g^n_{i+1,j,k}+g^{n+1}_{i-1,j,k}+g^n_{i,j+1,k}+g^{n+1}_{i,j-1,k}+g^n_{i,j,k+1}+g^{n+1}_{i,j,k-1}\right] \tag{9}$$

The standard five point leibman's formula for three coordinate axes is as presented in Eq. (9). This model was obtained from (8) through the

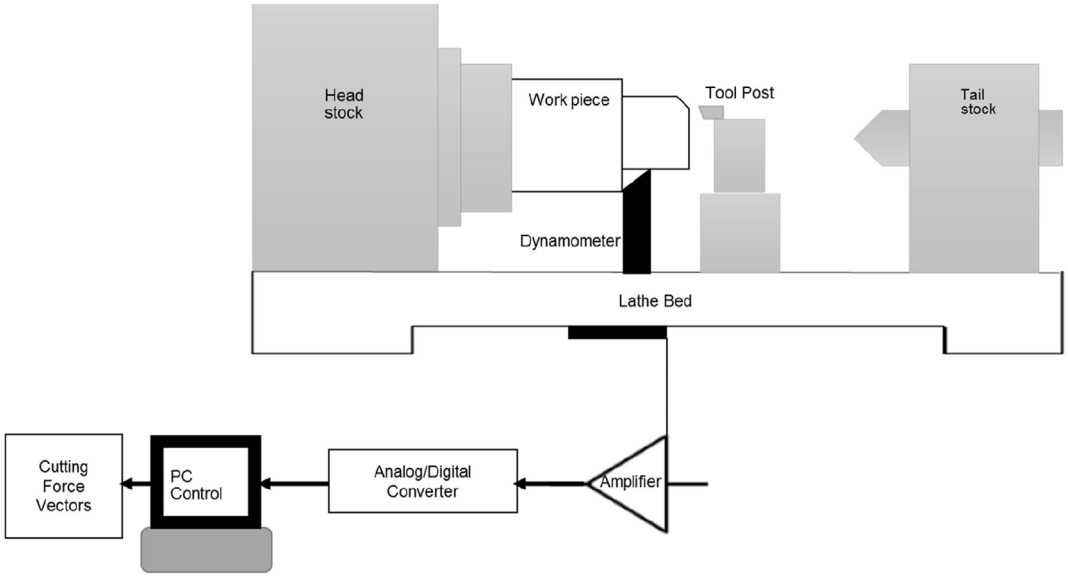

Figure 1. Schematic view of the experimental set-up.

Table 1. Experimental factors and levels Lin et al. (2001).

Level	Factor		
	(a) Depth of Cut (μm)	(b) Feed Rate (μm/rev)	(c) Cutting Speed (rpm)
1	0.350	0.080	86.120
2	0.800	0.200	121.580
3	1.250	0.320	202.630

Table 2. Design of experiment Lin et al. (2001).

Experiments	(a) Depth of Cut (μm)	(b) Feed Rate (μm/rev)	(c) Cutting Speed (rpm)
1: $a_1b_1c_1$	1.250	0.080	202.630
2: $a_1b_1c_2$	1.250	0.200	202.630
3: $a_1b_1c_3$	1.250	0.320	202.630
4: $a_1b_2c_1$	0.800	0.080	202.630
5: $a_1b_2c_2$	0.800	0.200	202.630
6: $a_1b_2c_3$	0.800	0.320	202.630
7: $a_1b_3c_1$	0.350	0.080	202.630
8: $a_1b_3c_2$	0.350	0.200	202.630
9: $a_1b_3c_3$	0.350	0.320	202.630
10: $a_2b_1c_1$	1.250	0.080	121.580
11: $a_2b_1c_2$	1.250	0.200	121.580
12: $a_2b_1c_3$	1.250	0.320	121.580
13: $a_2b_2c_1$	0.800	0.080	121.580
14: $a_2b_2c_2$	0.800	0.200	121.580
15: $a_2b_2c_3$	0.800	0.320	121.580
16: $a_2b_3c_1$	0.350	0.080	121.580
17: $a_2b_3c_2$	0.350	0.200	121.580
18: $a_2b_3c_3$	0.350	0.320	121.580
19: $a_3b_1c_1$	1.250	0.080	86.120
20: $a_3b_1c_2$	1.250	0.200	86.120
21: $a_3b_1c_3$	1.250	0.320	86.120
22: $a_3b_2c_1$	0.800	0.080	86.120
23: $a_3b_2c_2$	0.800	0.200	86.120
24: $a_3b_2c_3$	0.800	0.320	86.120
25: $a_3b_3c_1$	0.350	0.080	86.120
26: $a_3b_3c_2$	0.350	0.200	86.120
27: $a_3b_3c_3$	0.350	0.320	86.120

$L^F = 3^3$=(27 rows); 3 factors results in (3 columns).

combined effect of the difference equation and Gauss-Seidel's technique. Similarly, the five point "diagonal model" was developed from (8) and presented in (10). This was in turn translated to the vector form as presented in (11). The diagonal equation is often used for points at the vertex of Figure 3 or 4 usually without feasible solutions when (9) is utilised.

$$g(a,b,c)=\frac{1}{6}[g(a-\alpha,b-\beta,c)+g(a+\alpha,b-\beta,c)+g(a-\alpha,b+\beta,c) +g(a+\alpha,b+\beta,c)+g(a,b-\beta,c+\gamma)+g(a,b+\beta,c+\gamma)] \quad (10)$$

$$g_{i,j,k}=\frac{\varpi_i}{6}\left[g^{n+1}_{i-1,j-1,k}+g^{n}_{i+1,j-1,k}+g^{n}_{i-1,j+1,k}+g^{n}_{i+1,j+1,k}+g^{n}_{i,j-1,k+1}+g^{n}_{i,j+1,k+1}\right] \quad (11)$$

Where.

q= number of machining parameters

$g_{i,j,k}$ = point under consideration
$g^{n}_{i+1,j,k} = n^{th}$ iterative trial of point $g_{i+1,j,k}$in the +ve a-axis
$g^{n+1}_{i-1,j,k}= (n+1)^{th}$ iterative trial of point $g_{i-1,j,k}$ in the -ve a-axis
$g^{n}_{ij+1,k} = n^{th}$ iterative trial of point $g_{ij+1,k}$ in the +ve b-axis
$g^{n+1}_{i,j-1,k}= (n+1)^{th}$ iterative trial of point $g_{i,j-1,k}$ in the -ve b-axis
$g^{n}_{i,j,k+1} = n^{th}$ iterative trial of point$g_{i,j,k+1}$ in the +ve c-axis
$g^{n+1}_{i,j,k-1}= (n+1)^{th}$ iterative trial of point$g_{i,j,k-1}$in the -ve c-axis
$g^{n}_{i+1,j+1,k} = n^{th}$ iterative trial of point $g_{i+1,j+1,k}$ in the +ve a and b axes
$g^{n}_{i+1,j,k+1} = n^{th}$ iterative trial in the +ve a and c axes
ϖ_i = initialised weight; ϖ_{dd} = dynamic weight

3.1.1. Generalised models to determine the number of non-boundary points (off-ECC) for some selected levels and factors

[2 factors N-Levels]

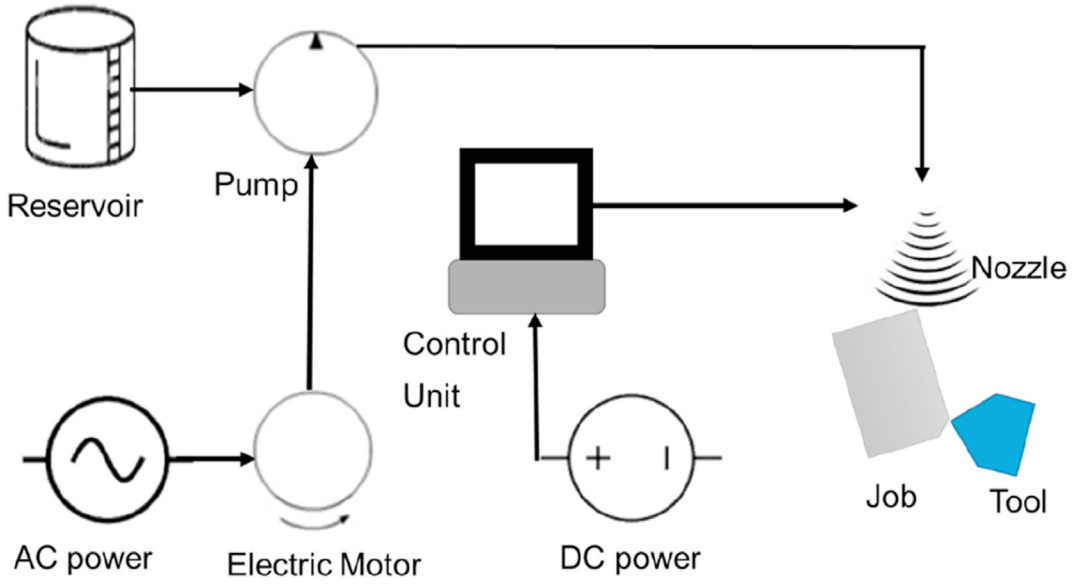

Figure 2. Schematic of the experimental set-up.

Table 3. Experimental factors and levels Mia et al. (2017).

Level	Factor		
	(a) Cutting Speed (m/min)	(b) Feed Rate (mm/rev)	(c) Flow Rate (ml/h)
1	66	0.18	1100
2	82	0.22	800
3	100	0.25	500

$$\sum_{j=2}^{m=2}\sum_{i=2}^{n=2}\left[A_{i,j}+A_{i,j+1}+A_{i,j+2}+\ldots+A_{i,\,N-1}\right]+\sum_{j=2}^{m=2}\times\sum_{i=3}^{n=3}\left[A_{i,j}+A_{i,j+1}+A_{i,j+2}+\ldots+A_{i,N-1}\right]+\sum_{j=2}^{m=2}\times\sum_{i=4}^{n=4}\left[A_{i,j}+A_{i,j+1}+A_{i,j+2}+\ldots+A_{i,N-1}\right]+\ldots+\sum_{j=2}^{m=2}\times\sum_{i=N-1}^{n=N-1}\left[A_{i,j}+A_{i,j+1}+A_{i,j+2}+\ldots+A_{i,N-1}\right] \quad (12)$$

[3 factors N-Levels] where N > 2

Note:

$A_{[Any\ subscript]}=1$; Hence $\left[A_{i,j}+A_{i,j,k}\right]=2$; $\left[A_{i,j+1,k}+A_{i,j,k+1}+A_{i,j+1,k+1}\right]=3$
$A_{i,j}+A_{i,j,k}+A_{i,j+1,k}+A_{i,j,k+1}+A_{i,j+1,k+1}=5$; $A_{i,j+1,k+1}=1$; $A_{i,j,k+1}=1$ (14)

$On\_ECC = L^F - Off\_ECC$
On_ECC = Cutting combinations on the edge of the mesh diagram.
Off_ECC = Cutting combinations off the edge of the mesh diagram.

$$\sum_{k=2}^{l=2}\sum_{j=2}^{m=2}\sum_{i=1}^{n=1}\left[\left(A_{i,j,k}+A_{i,j,k+1}+\ldots+A_{i,j,N-1}\right)+\left(A_{i,j+1,k}+A_{i,j+1,k+1}+\ldots+A_{i,j+1,N-1}\right)+\left(A_{i,j+2,k}+A_{i,j+2,k+1}+\ldots+A_{i,j+2,N-1}\right)+\ldots+\left(A_{i,N-1,k}+A_{i,N-1,k+1}+\ldots+A_{i,N-1,N-1}\right)\right]+\sum_{k=2}^{l=2}\sum_{j=2}^{m=2}\sum_{i=1}^{n=1}\left[\left(A_{i+1,j-1,k}+A_{i+1,j-1,k+1}+\ldots+A_{i+1,j-1,N-1}\right)+\left(A_{i+1,j,k-1}+A_{i+1,j,k}+A_{i+1,j,k+1}+\ldots+A_{i+1,j,N}\right)+\left(A_{i+1,j+1,k-1}+A_{i+1,j+2,k-1}+\ldots+A_{i+1,N-1,1}\right)+\left[\left(A_{i+1,j+1,k}\right)\right]+\left[\left(A_{i+1,j+1,k+1}+\ldots+A_{i+1,j+1,N-1}+A_{i+1,j+1,N}\right)\right]\right]+\ldots+\sum_{k=2}^{l=2}\sum_{j=2}^{m=2}\sum_{i=1}^{n=1}\left[\left(A_{i+1,N,k}+A_{i+1,N,k+1}\ldots+A_{i+1,N,N-1}\right)\right] \quad (13)$$

Table 4. Design of experiment Mia et al. (2017).

Experiments	(a) Depth of Cut (m/min)	(b) Feed Rate (mm/rev)	(c) Flow Rate (ml/h)
1: $a_1b_1c_1$	66	0.18	1100
2: $a_1b_1c_2$	66	0.18	800
3: $a_1b_1c_3$	66	0.18	500
4: $a_1b_2c_1$	66	0.22	1100
5: $a_1b_2c_2$	66	0.22	800
6: $a_1b_2c_3$	66	0.22	500
7: $a_1b_3c_1$	66	0.25	1100
8: $a_1b_3c_2$	66	0.25	800
9: $a_1b_3c_3$	66	0.25	500
10: $a_2b_1c_1$	82	0.18	1100
11: $a_2b_1c_2$	82	0.18	800
12: $a_2b_1c_3$	82	0.18	500
13: $a_2b_2c_1$	82	0.22	1100
14: $a_2b_2c_2$	82	0.22	800
15: $a_2b_2c_3$	82	0.22	500
16: $a_2b_3c_1$	82	0.25	1100
17: $a_2b_3c_2$	82	0.25	800
18: $a_2b_3c_3$	82	0.25	500
19: $a_3b_1c_1$	100	0.18	1100
20: $a_3b_1c_2$	100	0.18	800
21: $a_3b_1c_3$	100	0.18	500
22: $a_3b_2c_1$	100	0.22	1100
23: $a_3b_2c_2$	100	0.22	800
24: $a_3b_2c_3$	100	0.22	500
25: $a_3b_3c_1$	100	0.25	1100
26: $a_3b_3c_2$	100	0.25	800
27: $a_3b_3c_3$	100	0.25	500

$L^F = 3^3$=(27 rows); 3 factors results in (3 columns).

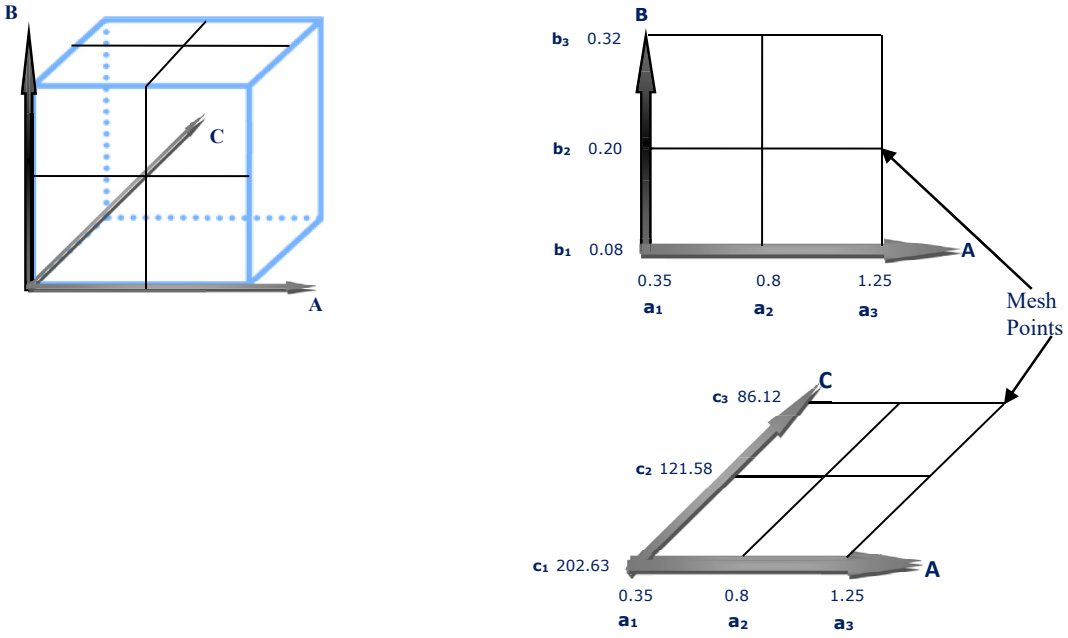

Figure 3. Mesh diagram for interacting machining parameters in Table 2.

3.1.2. *Computerized pseudo-code to generate all twenty-seven points in the sample space as presented in the appendices using dynamic weights*

/// m= (number of experimental factors)

$$a_{i+1}b_{j+1}c_{k+i}{}^{(n+1)} = \left[1/6^{*}\left[a_ib_{j+1}c_{K+1}{}^{(n+1)} + a_{i+2}b_{j+1}c_{K+1}{}^{(n)} + a_{i+1}b_jc_{K+1}{}^{(n+1)} + a_{i+1}b_{j+2}c_{K+1}{}^{(n)} + a_{i+1}b_{j+1}c_K{}^{(n+1)} + a_{i+1}b_{j+1}c_{K+2}{}^{(n)}\right]\right]^{*}w_{dd}$$

```
For: i=0 to m-1
j=0 to m-1
k=0 to m-1
next k
next j
next i
if i=j=k then end ///
```

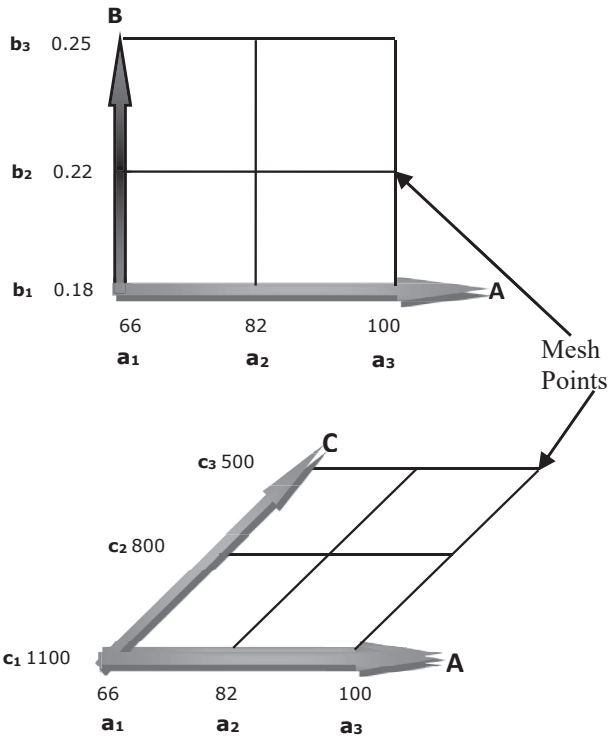

Figure 4. Mesh diagram for interacting machining parameters in Table 4.

Figures 3 and 4 both represent diagrammatic views of the machining parameters in 2D and 3D outlooks. While Figure 3 depicts the cutting parameters presented in Table 2, Figure 4 represents the cutting parameters presented in Table 3.

These figures basically serve as graphical links between the difference analysis algorithm and the experimental parameters and outputs. The proposed difference analysis modelling procedure is premised on the use of mesh diagrams as presented in Figures 3 and 4 for mapping and ease of vector points tracking.

Figure 5 presents an operational feedback loop that connects the experimental outputs to the difference analysis algorithm. It further elucidates the process of adaptive weight generation for accuracy enhancement of surface roughness prediction related to the Off-ECC points i.e. points that are off the edges or vertices of the mesh diagram presented in Figure 3 or 4. By default, each Off-ECC points is iterated until the actual response captured by the estimator is greater than or equal to the desired/experimental surface roughness reading (set point). At the point of stability, a zero output response takes place at the comparator level. The discrepancy between the predicted surface roughness and the desired, serves as a driving mechanism for the operation of the adaptive weight algorithm prior to attainment of a steady state condition by the Off-ECC points. This action of the adaptive weights is often characterised by weight gains or losses as presented in Figure 5.

3.1.3. Feedback loop for dynamic weight scheme

The adaptive weight concept presented in this research is premised on feedback from iterations linked to Figure 5. The pseudo-code below presents the activities in the feedback loop.

1.Initialize counter = 0.
2.Initialize: Surface roughness prediction reading $g[x_i y_j z_k]=0$
3.Set iterative trial limit [m] epoch
4. If counter > 0 for counter = [0 to m] then
5. Initialize weight $\varpi_i>0$ for all Off-ECC points
6.Input experimental surface readings(set-points for On-ECC points]
7a.Compute g $[a_ib_jc_k]=1/6\ [a_{i-1}b_jc_k + a_{i+1}b_jc_k + a_ib_{j-1}c_k + a_ib_{j+1}c_k + a_ib_jc_{k-1}+a_ib_jc_{k+1}]*\varpi_i$ [computation for mid-points in the mesh viz:(standard five points difference analysis] or
7b.Compute g $[a_ib_jc_k]= 1/6\ [a_{i-1}b_{j-1}c_k + a_{i+1}b_{j-1}c_k + a_{i-1}b_{j+1}c_k + a_{+1}b_{j+1}c_k + a_ib_{j-1}c_{k+1} + a_ib_{j+1}c_{k+1}]*\varpi_i$ [five point diagonal analysis: only for selected mesh points that cannot be addressed using the algorithm in [7a]; counter=counter + 1
8.If g $[a_ib_jc_k]$>= set-point
9.Compute new weight $[\varpi_{dd}]=(\text{set-point}*\varpi_i)/g[a_ib_jc_k]$
10a.g $[a_ib_jc_k]=1/6\ [a_{i-1}b_jc_k+a_{i+1}b_jc_k+a_ib_{j-1}c_k+a_ib_{j+1}c_k+a_ib_jc_{k-1}+a_ib_jc_{k+1}]*\varpi_{dd}$ or
10b. g $[a_ib_jc_k]=1/6\ [a_{i-1}b_{j-1}c_k+a_{i+1}b_{j-1}c_k+a_{i-1}b_{j+1}c_k\ +a_{+1}b_{j+1}c_k+a_ib_{j-1}c_{k+1}+a_ib_{j+1}c_{k+1}]*\varpi_{dd}$
11. If step [8] is not, repeat step (7a or 7b) until step [8] is then compute [9], [10a or 10b]
12. End.

3.1.4. Initial weight selection procedure

The initial weight assignment process is often commenced with a zero "0" initialisation. Hence, both the surface roughness values and initial weights are tuned to zero at iteration zero. Subsequently in iteration one, the chosen initial weights become active and these by default, should be greater than zero via a bottom-up numerical sequence assignment approach. Usually, a value of "0.1" can be a good starting point for initial

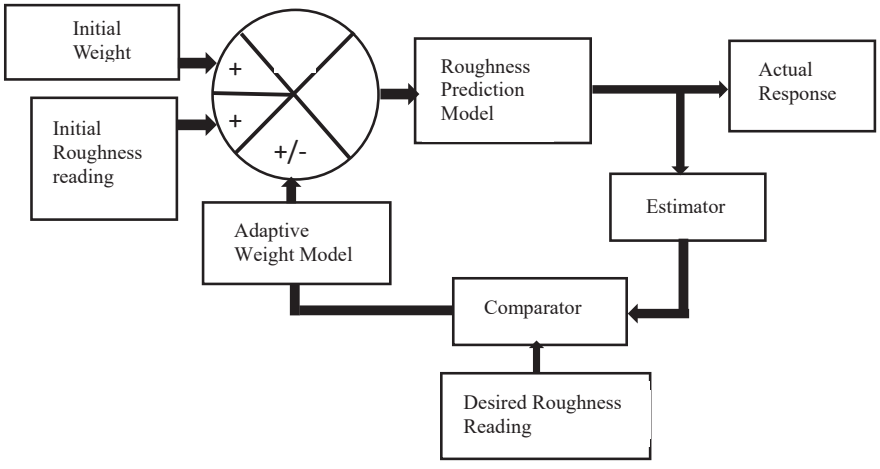

Figure 5. Feedback loop for computation of adaptive weight ϖ_{dd}

Table 5. Computed Surface Roughness Readings for Off-ECC sub-category Machining Parameters.

[Off-ECC]/Surface Roughness	Iterations								
	1	2	3	4	5	6	7	8	9
	$a_1b_2c_2 = 0.649$ $w_1 = 1.022$	$a_1b_2c_2 = 2.502$ $w_1 = 1.022$	$a_1b_2c_2 = 2.601$ $w_1 = 1.022$	$a_1b_2c_2 = 2.797$ $w_1 = 1.022$	$a_1b_2c_2 = 3.096$ $w_1 = 1.022$	$a_1b_2c_2 = 3.341$ $w_{11} = 1.013$	$a_1b_2c_2 = 3.341$ $w_{11} = 1.005$	$a_1b_2c_2 = 3.341$ $w_{11} = 1.002$	$a_1b_2c_2 = 3.341$ $w_{11} = 1.002$
	$a_2b_1c_2 = 0.199$ $w_2 = 0.740$	$a_2b_1c_2 = 0.419$ $w_2 = 0.740$	$a_2b_1c_2 = 0.449$ $w_2 = 0.740$	$a_2b_1c_2 = 0.531$ $w_2 = 0.740$	$a_2b_1c_2 = 0.652$ $w_2 = 0.740$	$a_2b_1c_2 = 0.838$ $w_{22} = 0.737$	$a_2b_1c_2 = 0.838$ $w_{22} = 0.722$	$a_2b_1c_2 = 0.838$ $w_{22} = 0.716$	$a_2b_1c_2 = 0.838$ $w_{22} = 0.716$
	$a_2b_2c_1 = 0.667$ $w_3 = 1.022$	$a_2b_2c_1 = 2.639$ $w_3 = 1.022$	$a_2b_2c_1 = 2.681$ $w_3 = 1.022$	$a_2b_2c_1 = 2.794$ $w_3 = 1.022$	$a_2b_2c_1 = 2.961$ $w_3 = 1.022$	$a_2b_2c_1 = 3.224$ $w_3 = 1.022$	$a_2b_2c_1 = 3.247$ $w_{33} = 1.022$	$a_2b_2c_1 = 3.247$ $w_{33} = 1.019$	$a_2b_2c_1 = 3.247$ $w_{33} = 1.019$
	$a_2b_2c_2 = 0.248$ $w_4 = 0.981$	$a_2b_2c_2 = 0.909$ $w_4 = 0.981$	$a_2b_2c_2 = 1.892$ $w_4 = 0.981$	$a_2b_2c_2 = 3.431$ $w_4 = 0.981$	$a_2b_2c_2 = 3.571$ $w_4 = 0.981$	$a_2b_2c_2 = 3.630$ $w_{44} = 0.955$	$a_2b_2c_2 = 3.630$ $w_{44} = 0.952$	$a_2b_2c_2 = 3.630$ $w_{44} = 0.952$	$a_2b_2c_2 = 3.630$ $w_{44} = 0.952$
	$a_2b_2c_3 = 0.818$ $w_5 = 1.190$	$a_2b_2c_3 = 3.067$ $w_5 = 1.190$	$a_2b_2c_3 = 3.154$ $w_{55} = 1.151$	$a_2b_2c_3 = 3.154$ $w_{55} = 1.190$	$a_2b_2c_3 = 3.154$ $w_{55} = 1.044$	$a_2b_2c_3 = 3.154$ $w_{55} = 1.041$	$a_2b_2c_3 = 3.154$ $w_{55} = 1.041$	$a_2b_2c_3 = 3.154$ $w_{55} = 1.041$	$a_2b_2c_3 = 3.154$ $w_{55} = 1.041$
	$a_2b_3c_2 = 4.199$ $w_6 = 1.545$	$a_2b_3c_2 = 8.503$ $w_{66} = 1.500$	$a_2b_3c_2 = 8.503$ $w_{66} = 1.457$	$a_2b_3c_2 = 8.503$ $w_{66} = 1.396$	$a_2b_3c_2 = 8.503$ $w_{66} = 1.391$	$a_2b_3c_2 = 8.503$ $w_{66} = 1.388$	$a_2b_3c_2 = 8.503$ $w_{66} = 1.388$	$a_2b_3c_2 = 8.503$ $w_{66} = 1.388$	$a_2b_3c_2 = 8.503$ $w_{66} = 1.388$
	$a_3b_2c_2 = 0.824$ $w_7 = 1.116$	$a_3b_2c_2 = 3.290$ $w_7 = 1.116$	$a_3b_2c_2 = 3.473$ $w_7 = 1.116$	$a_3b_2c_2 = 3.759$ $w_7 = 1.116$	$a_3b_2c_2 = 3.785$ $w_7 = 1.116$	$a_3b_2c_2 = 3.794$ $w_{77} = 1.115$	$a_3b_2c_2 = 3.794$ $w_{77} = 1.115$	$a_3b_2c_2 = 3.794$ $w_{77} = 1.115$	$a_3b_2c_2 = 3.794$ $w_{77} = 1.115$
							⇦ Global stability attained		

weight selection of all points to be predicted. However, this is mere advisory since any value above "0" will initiate the iteration process. Once the iterative process commences, the need to adjust initial weights comes to play for different prediction points due to non-convergence of one or more set-points irrespective of the number of epochs or iterations. In such a scenario, the initial weights must be adjusted for the non-converging points only. This can be done by applying incremental values of "0.1" or lesser values until an iterative convergence is achieved for the non-converging points. While non-convergence is often associated with the choice of very low initial weights, large initial weight values can result in "set point/s overshoot". However, this is often with little or no effect as the set points by default act as truncating mechanism to bring back all overshoots to the desired level. Hence, issues associated with non-convergence basically emanate from small values of initial weights. A steady state condition is said to have been attained during simulation trials once the predicted and experimented surface roughness values i.e. the set-points have converged. The system of weights i.e. initial and dynamic weights are synchronised to work simultaneously in the developed integrated model. The initial weights only transform into dynamic weights at the point of convergence hence $\overline{\omega}_i$ becomes $\overline{\omega}_{dd}$. In some instances, after attaining convergence, the dynamic weights may change in value in order to sustain the attained convergence. This occurs when one or more points in the prediction chain are yet to attain convergence.

4. Results and discussion

The virtual experiments conducted in this research were effected using Matlab R2014b software. A priori knowledge of cutting combinations and corresponding surface roughness readings formed major requirements for the simulation trials. The surface roughness readings were used as set-points for the determination of a set of synchronised dynamic weights for prediction of surface roughness readings for different cutting combinations of interest. The simulation exercise is divided into two sub-phases viz: prediction of surface roughness readings for points off the edge of the mesh diagram in Figures 3 and 4 referred to as off-edge cutting combinations (Off-ECC). The second sub-phase is the recovery of points on the edges of the mesh diagram also referred to as on edge cutting combinations (On-ECC). The notations (a_i, b_j, c_k) as utilised in this research to depict different combination of factors for the machining process represents the depth of cut, feed rate and cutting speed respectively for the first experimental data as presented in Tables 1, 2, and 6 while same notations depict depth of cut, feed rate and flow rate in the second experimental data as presented in Tables 3, 4, and 8. Also, the associated subscripts (i, j, k) respectively represents levels: 1, 2 and 3 as shown in Tables 1, 2, 3, and 4. When a cutting combination features a subscript of "$_2$" for only one of subscripts (i, j, k), that point on the 3D mesh is classified as on the edge cutting combination (On-ECC). However, when a cutting combination features the subscript "$_2$" for at least two of the subscripts (i,j,k), it implies that it is a point off the edge on the 3D mesh i.e (Off-ECC). The experimental sample space, premised on the design of experiment has twenty outputs associated with the (On-ECC) in both experimental scenarios viz: $[a_1,b_1,c_1;\ a_1,b_1,c_2;\ a_1,b_1,c_3; a_1,b_2,c_1; a_1,b_2,c_2; a_1,b_2,c_3; a_1,b_3,c_1;\ a_1,b_3,c_2; a_1,b_3,c_3; a_2,b_1,c_1; a_2,b_1,c_3; a_2,b_3,c_1; a_2,b_3,c_2; a_2,b_3,c_3; a_3,b_1,c_1; a_3,b_1,c_2; a_3,b_1,c_3; a_3,b_2,c_1; a_3,b_2,c_3; a_3,b_3,c_1; a_3,b_3,c_2;\ a_3,b_3,c_3]$. However, seven cutting combinations are associated with the (Off-ECC) viz: $a_1,b_2,c_2;\ a_2,b_1,c_2;\ a_2,b_2,c_1;\ a_2,b_2,c_2;\ a_2,b_2,c_3; a_2,b_3,c_2$ and a_3,b_2,c_2.

4.1. Predictions & experimental datasets

This sub-section presents a discussion of the predictive results as contained in Table 5 and. 6. The predictive iterations for all seven points referred to as (Off-ECC) was characterised with random selection of initialised weights $(\overline{\omega}_i)$ within the range of "0.7 and 1.6" as numbers within this range facilitated convergence of all the seven

Table 6. Experimental and Computational Results for Surface Roughness Considering Proposed and some Earlier Techniques.

S/N	[a] Depth of cut (mm)	[b] Feed rate (mm/rev)	[c] Cutting speed (m/min)	Expt. value (μm)	Abductive network *Predicted value(μm)* Lin et al. (2001)	Percentage error (%) Lin et al. (2001)	Regression analysis Predicted value (μm) Lin et al. (2001)	Percentage error (%) Lin et al. (2001)	Proposed Difference Analysis and Feedback control Technique (μm)
1	1.250	0.080	202.630	0.8480	0.940	10.850	1.060	25.000	$a_3b_1c_3 = 0.848$
2	1.250	0.200	202.630	3.1110	3.130	0.610	3.460	11.220	$a_3b_2c_3 = 3.111$
3	1.250	0.320	202.630	8.2790	8.200	0.950	8.200	0.950	$a_3b_3c_3 = 8.279$
4	0.800	0.080	202.630	1.0650	1.070	0.470	0.920	13.620	$a_2b_1c_3 = 1.065$
5	0.800	0.200	202.630	3.1540	2.960	6.150	3.110	1.400	$a_2b_2c_3 = 3.154$
6	0.800	0.320	202.630	7.5680	7.700	1.740	7.640	0.950	$a_2b_3c_3 = 7.568$
7	0.350	0.080	202.630	1.0870	1.170	7.640	0.780	28.240	$a_1b_1c_3 = 1.087$
8	0.350	0.200	202.630	2.8130	2.740	2.600	2.760	1.880	$a_1b_2c_3 = 2.813$
9	0.350	0.320	202.630	7.0040	7.160	2.230	7.090	1.230	$a_1b_3c_3 = 7.004$
10	1.250	0.080	121.580	0.7150	0.780	9.090	1.140	59.440	$a_3b_1c_2 = 0.715$
11	1.250	0.200	121.580	3.7940	3.880	2.270	3.910	3.060	$a_3b_2c_2 = 3.794$
12	1.250	0.320	121.580	9.4890	9.340	1.570	9.010	5.050	$a_3b_3c_2 = 9.489$
13	0.800	0.080	121.580	0.8380	0.820	2.150	1.000	19.330	$a_2b_1c_2 = 0.838$
14	0.800	0.200	121.580	3.6300	3.600	0.830	3.560	1.930	$a_2b_2c_2 = 3.630$
15	0.800	0.320	121.580	8.5030	8.680	2.080	8.450	0.620	$a_2b_3c_2 = 8.503$
16	0.350	0.080	121.580	0.7550	0.830	9.930	0.870	15.230	$a_1b_1c_2 = 0.755$
17	0.350	0.200	121.580	3.3410	3.290	1.530	3.210	3.920	$a_1b_2c_2 = 3.341$
18	0.350	0.320	121.580	7.9430	7.990	0.590	7.900	0.540	$a_1b_3c_2 = 7.943$
19	1.250	0.080	86.120	0.7270	0.710	2.340	0.750	3.160	$a_3b_1c_1 = 0.727$
20	1.250	0.200	86.120	3.4660	3.500	0.980	3.680	6.170	$a_3b_2c_1 = 3.466$
21	1.250	0.320	86.120	9.0310	8.870	1.780	8.930	1.120	$a_3b_3c_1 = 9.031$
22	0.800	0.080	86.120	0.8580	0.830	3.260	0.620	27.740	$a_2b_1c_1 = 0.858$
23	0.800	0.200	86.120	3.2470	3.270	0.710	3.330	2.560	$a_2b_2c_1 = 3.247$
24	0.800	0.320	86.120	8.1150	8.210	1.170	8.380	3.270	$a_2b_3c_1 = 8.115$
25	0.350	0.080	86.120	0.9000	0.910	1.110	0.480	46.670	$a_1b_1c_1 = 0.900$
26	0.350	0.200	86.120	3.0550	3.010	0.600	2.980	2.450	$a_1b_2c_2 = 3.055$
27	0.350	0.320	86.120	7.5550	7.540	0.200	7.820	3.510	$a_1b_3c_1 = 7.555$

iterations. Details on initial weight selection procedure is contained in section 3.1.2. Table 5 presents both the transient and steady state dynamic weights and predicted surface roughness for all seven points depicted as Off-ECC. Iteration one as presented in Table 5 is absolutely transient behaved. This can be seen across-board all seven Off-ECC machining combinations listed. A steady-state condition for

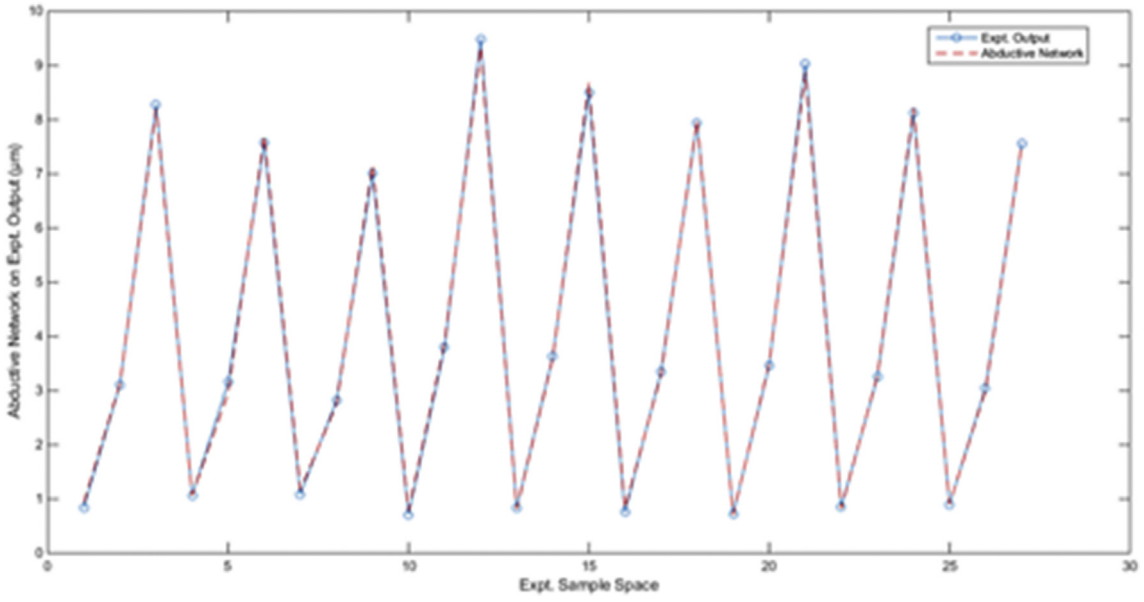

Figure 6. A graph comparing experimental output and abductive network.

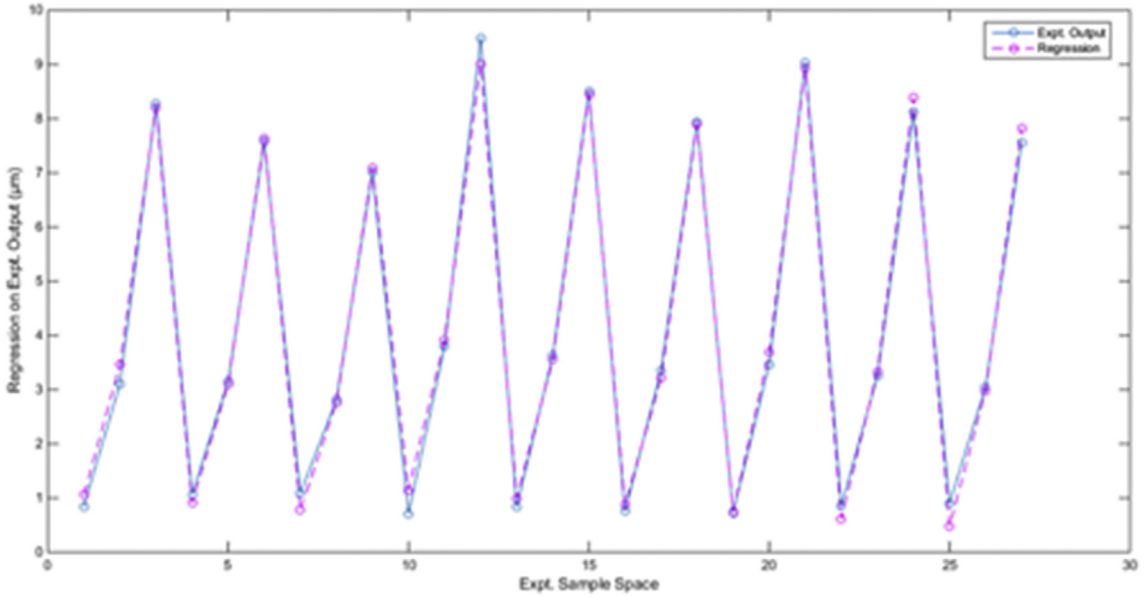

Figure 7. A graph comparing experimental output and regression analysis.

machining parameter a_2, b_3, c_2 was attained in iteration 2. However, the dynamic weight adjustment continued up until the fifth iteration without changing the surface roughness reading. This is premised on the fact that the predictive models are tightly coupled hence the generated weights are affected by the transient behaviour of other cutting combinations within the connected system of models. a_2, b_3, c_2

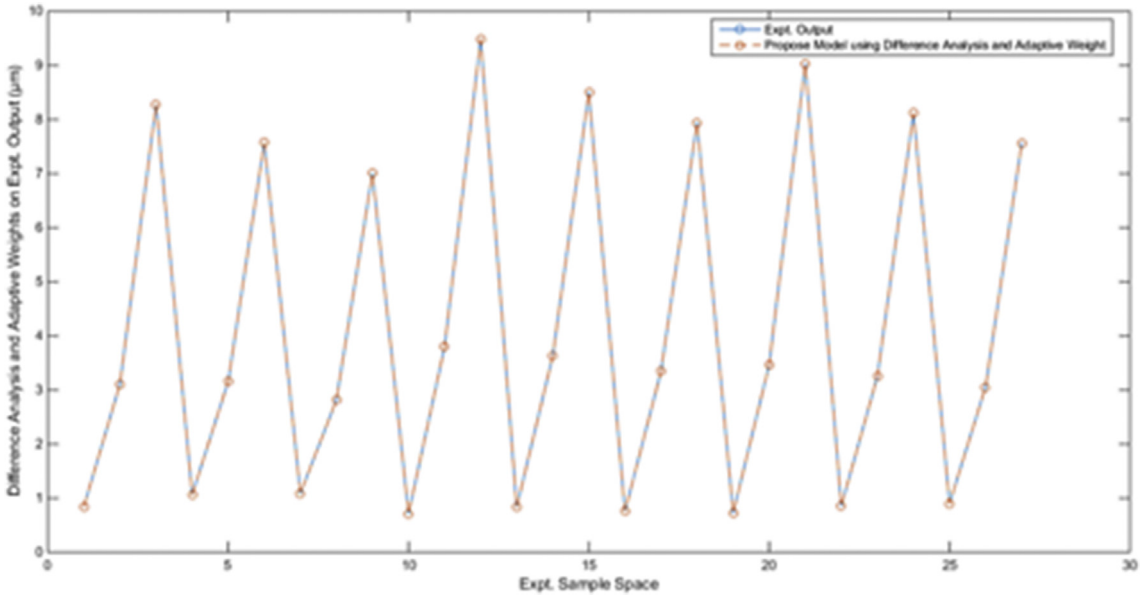

Figure 8. A graph comparing experimental output and proposed approach.

Table 7. Computed Surface Roughness Readings for Machining Parameters of the Off-ECC sub-category.

Iterations								
1	$a_1b_2c_2 = 1.566$ $w_1 = 1.500$	$a_2b_1c_2 = 0.925$ $w_2 = 1.200$	$a_2b_2c_1 = 0.997$ $w_3 = 1.300$	$a_2b_2c_2 = 0.872$ $w_4 = 1.500$	$a_2b_2c_3 = 1.627$ $w_5 = 1.400$	$a_2b_3c_2 = 1.360$ $w_6 = 1.300$	$a_3b_2c_2 = 1.237$ $w_7 = 1.300$	
2	$a_1b_2c_2 = 2.717$ $w_{11} = 1.064$	$a_2b_1c_2 = 2.387$ $w_{22} = 1.111$	$a_2b_2c_1 = 2.350$ $w_{33} = 1.168$	$a_2b_2c_2 = 2.817$ $w_{44} = 1.041$	$a_2b_2c_3 = 3.220$ $w_{55} = 1.272$	$a_2b_3c_2 = 2.825$ $w_{66} = 1.199$	$a_3b_2c_2 = 2.743$ $w_{77} = 1.219$	⟸ Global stability attained
3	$a_1b_2c_2 = 2.717$ $w_{11} = 1.064$	$a_2b_1c_2 = 2.387$ $w_{22} = 1.111$	$a_2b_2c_1 = 2.350$ $w_{33} = 1.168$	$a_2b_2c_2 = 2.817$ $w_{44} = 1.041$	$a_2b_2c_3 = 3.220$ $w_{55} = 1.272$	$a_2b_3c_2 = 2.825$ $w_{66} = 1.199$	$a_3b_2c_2 = 2.743$ $w_7 = 1.219$	

Table 8. Experimental and Computational Results for Surface Roughness Considering Proposed and some Earlier Techniques.

S/N	[a] Cutting Speed (m/min)	[b] Feed rate (mm/rev)	[c] Flow Rate (ml/h)	Expt. value (μm)	Artificial Neural Network *Prediction value(μm)* Mia et al. (2017b)	Absolute Percentage error (%) Mia et al. (2017b)	Proposed Difference Analysis and Feedback control Technique
1: $a_1b_1c_1$	66	0.18	1100	2.173	2.17	0.35	2.173
2: $a_1b_1c_2$	66	0.18	800	2.438	2.44	0.13	2.438
3: $a_1b_1c_3$	66	0.18	500	2.838	2.84	0.18	2.838
4: $a_1b_2c_1$	66	0.22	1100	2.416	2.38	1.65	2.416
5: $a_1b_2c_2$	66	0.22	800	2.717	2.73	0.63	2.717
6: $a_1b_2c_3$	66	0.22	500	3.270	3.18	2.84	3.27
7: $x_1y_3z_1$	66	0.25	1100	2.613	2.61	0.28	2.613
8: $x_1y_3z_2$	66	0.25	800	2.972	2.94	1.10	2.972
9: $x_1y_3z_3$	66	0.25	500	3.350	3.34	0.42	3.350
10: $x_2y_1z_1$	82	0.18	1100	2.187	2.15	1.64	2.187
11: $x_2y_1z_2$	82	0.18	800	2.387	2.46	3.21	2.387
12: $x_2y_1z_3$	82	0.18	500	2.829	2.87	1.61	2.829
13: $x_2y_2z_1$	82	0.22	1100	2.350	2.30	2.20	2.350
14: $x_2y_2z_2$	82	0.22	800	2.817	2.71	3.92	2.817
15: $x_2y_2z_3$	82	0.22	500	3.220	3.19	0.84	3.220
16: $x_2y_3z_1$	82	0.25	1100	2.432	2.52	3.67	2.432
17: $x_2y_3z_2$	82	0.25	800	2.825	2.94	4.23	2.825
18: $x_2y_3z_3$	82	0.25	500	3.163	3.40	7.50	3.163
19: $x_3y_1z_1$	100	0.18	1100	2.321	2.20	5.26	2.321
20: $x_3y_1z_2$	100	0.18	800	2.617	2.56	2.36	2.617
21: $x_3y_1z_3$	100	0.18	500	2.926	2.91	0.42	2.926
22: $x_3y_2z_1$	100	0.22	1100	2.218	2.29	3.07	2.218
23: $x_3y_2z_2$	100	0.22	800	2.743	2.72	0.75	2.743
24: $x_3y_2z_3$	100	0.22	500	3.105	3.17	1.97	3.105
25: $x_3y_3z_1$	100	0.25	1100	2.672	2.47	7.60	2.672
26: $x_3y_3z_2$	100	0.25	800	2.749	2.95	7.45	2.749
27: $x_3y_3z_3$	100	0.25	500	3.470	3.40	1.92	3.470

represents the cutting parameters (0.800, 0.320, 121.580) i.e. depth of cut, feed rate and cutting speed. A steady-state condition for machining parameters a_2, b_2, c_3 was attained at the end of the 3rd iteration. However, as in the previous case, the weight remained transient until the fifth iteration. This represents experimental combination (0.800, 0.200, 202.630) which implies the depth of cut, feed rate and cutting speed. Furthermore, iterations 4 and 5 in Table 5 attained a state of stability for surface roughness.

prediction of cutting combinations: a_1, b_2, c_2; a_2, b_1, c_2; a_2, b_2, c_2 and a_3, b_2, c_2 depicting (0.350, 0.200, 121.580), (0.800, 0.080, 121.580), (0.800, 0.200, 121.580) and (1.250, 0.200, 121.580) respectively as presented in Table 6. Machining combination a_2, b_2, c_1 associated with

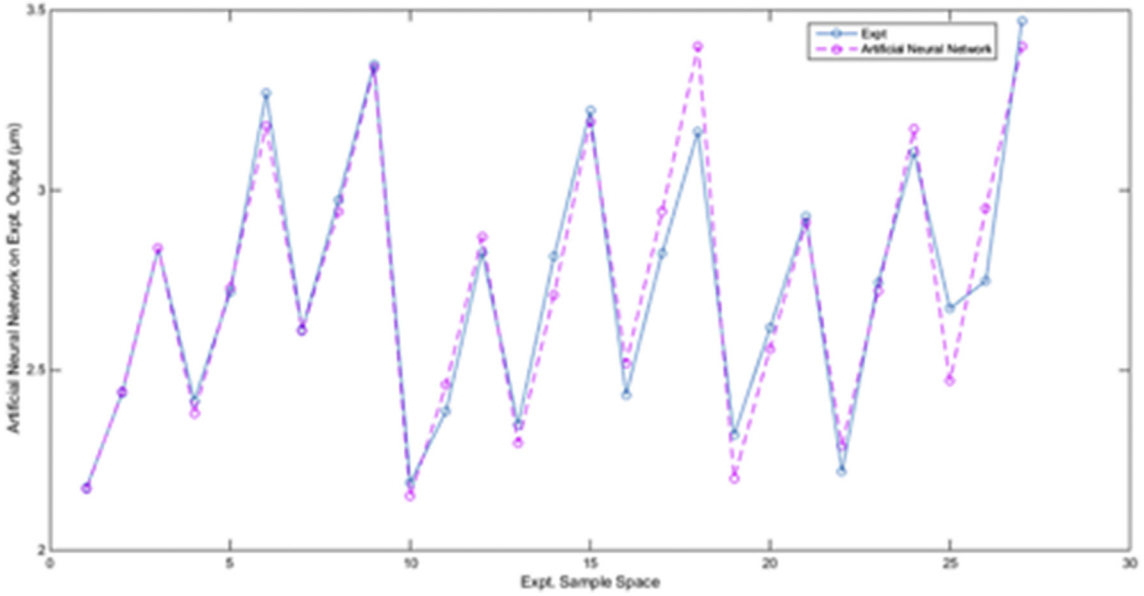

Figure 9. A graph comparing experimental output and artificial neural network.

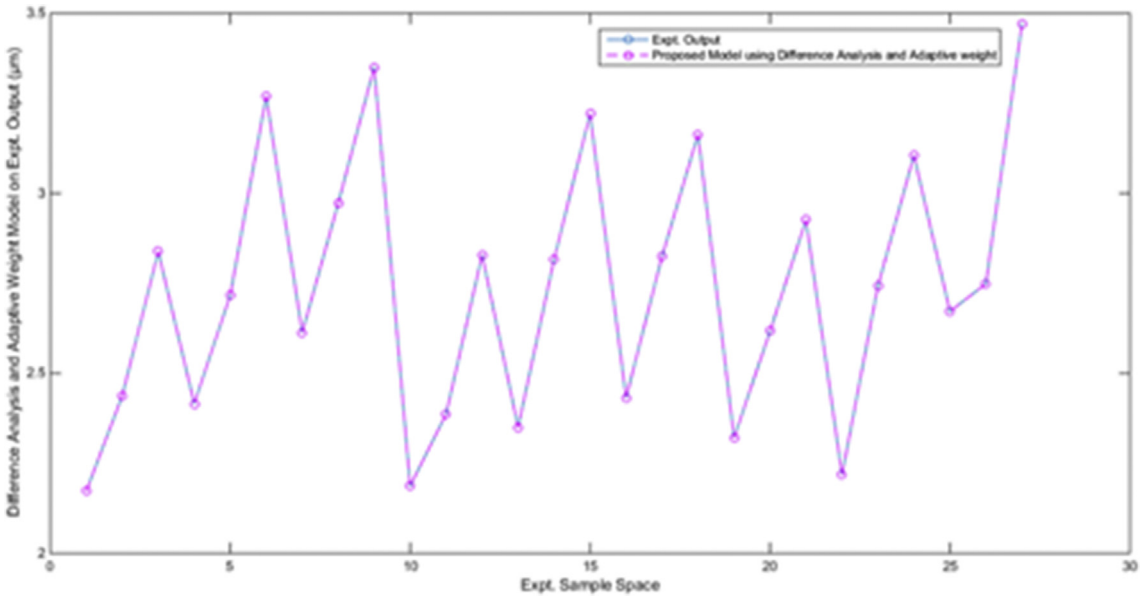

Figure 10. A graph comparing experimental output and the proposed approach.

Table 9. ANOVA computation for dataset in Table 2.

SUMMARY						
Groups	Count	Sum	Average	Variance		
Depth of Cut (μm)	27	21.6	0.8	0.14		
Feed Rate (μm/rev	27	5.4	0.2	0.01		
Cutting Speed (rpm)	27	3693	137	2469		
ANOVA						
Source of Variation	SS	df	MS	F	P-value	F crit
Between Groups	334289	2	167144	203.05	1.2*10-31	3.11
Within Groups	64207	78	823			
Total	39850	80				

experimental values (0.800, 0.200, 86.120) only attained a steady-state condition at the end of the 7th iteration. The 8th and 9th iterations showed stability attainment in both weight variation and surface roughness prediction.

The mean squared error estimation carried out on the predictive outcomes are as contained in Table 6. Furthermore, Figures 6, 7, and 8 present graphical plots comparing the respective approaches with experimental outcomes. Specifically, Figure 6 presents a comparison of the outputs between the experimental and Abductive Network outputs while Figure 7 presents a comparison between the outputs from experimentation and regression analysis. Furthermore, Figure 8 presents a comparison between the proposed hybrid model and the experimental results. Figure 6 had a reduced graphical discrepancy between the predicted and experimented relative to Figure 7 while Figure 8 presents an absolute trend match between the computational and experimental outputs. The numeric discrepancies of these results are as presented in Table 6. In a sequential order of algorithmic effectiveness, the least effective technique amongst the three techniques compared is the Regression analysis method. This was followed by the Abductive network method and lastly the proposed hybrid scheme of difference analysis method and feedback controlled technique with zero error margin.

Table 10. ANOVA computation for dataset in Table 4.

SUMMARY						
Groups	Count	Sum	Average	Variance		
Cutting Speed (m/min)	27	2232	82.67	200.31		
Feed Rate (mm/rev)	27	5.85	0.22	8.5* 10-4		
Flow Rate (ml/h)	27	21600	800	6.2* 104		
ANOVA						
Source of Variation	SS	df	MS	F	P-value	F crit
Between Groups	1.0* 107	2	5224583	250.75	1.0*10-34	3.11
Within Groups	1.6*106	78	20836			
Total	1.2*107	80				

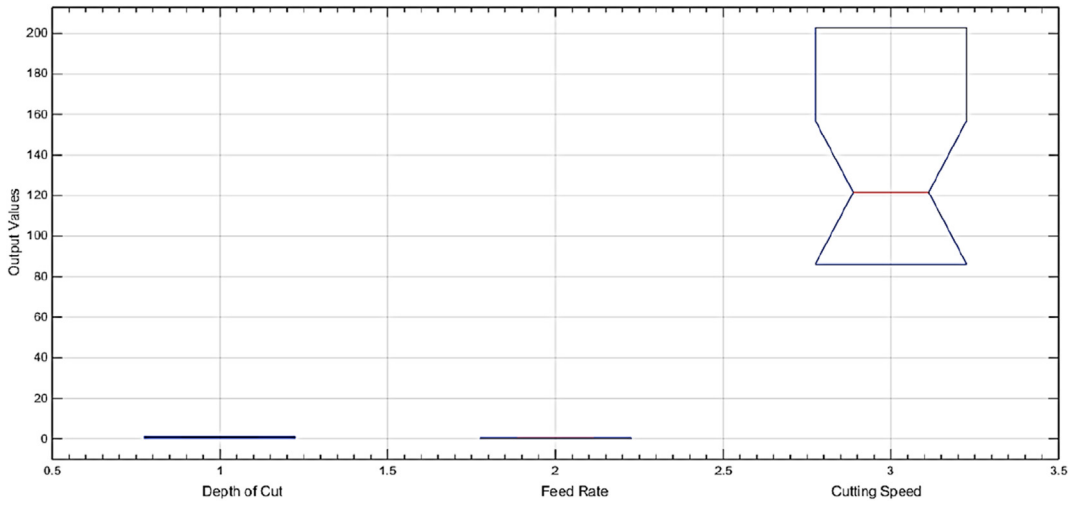

Figure 11. Box notch diagram for experimental data in Table 2.

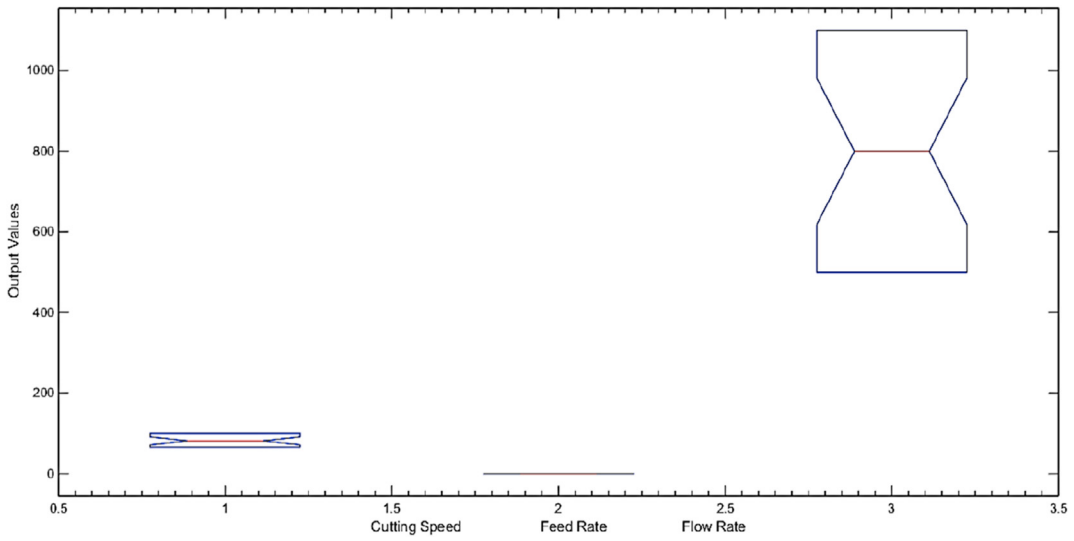

Figure 12. Box notch diagram for experimental data in Table 4.

4.2. *Predictions & experimental datasets: Tables 7 and 8*

This sub-section presents a discussion on the predictive results as contained in Tables 7 and 8. The predictive iterations for all seven points referred to as (Off-ECC) were characterised with random selection of initialised weights ($\overline{\omega}_i$) within the range of "1.2 and 1.5" as numbers within this range facilitated convergence of all the seven iterations. A steady-state condition was attained in Table 7 for all predictive machining combinations at the end of the second iteration: These points include $a_1, b_2, c_2(66, 0.22, 800)$; $a_2, b_1, c_2(82, 0.18, 800)$; a_2, b_2, c_1 (82, 0.22,1100); $a_2, b_2, c_2(82, 0.22, 800)$; $a_2, b_2, c_3(82, 0.22, 500)$; a_2, b_3, c_2 (82, 0.25,800) and. a_2, b_2, c_3 (82,0.22,500). Unlike in the previous predictive exercise in Table 5, the convergence herein was faster due to increased values for initial weights assignment. The mean absolute percentage error for these predictions are as presented in Table 8 with the proposed approach recording zero error discrepancy between the experimental and predicted datasets. Furthermore, Figures 9 and 10 present graphical plots comparing outputs from the use of Artificial Neural Networks and the proposed hybrid scheme of difference analysis and dynamic weights feedback system. Synonymous to the error computations in Table 8, Figure 9 showed a higher level of discrepancy between the predicted and experimented relative to Figure 10 which presents an absolute trend match between the computational and experimental outputs. The Supplementary Material (Appendices) presents Appendix A, a breakdown of the models representing the (Off-ECC) points on the mesh. Furthermore, the surface roughness readings for the On-ECC points previously used as set-points for the prediction of surface roughness of the Off-ECC points, were recovered using the proposed adaptive modelling scheme. The elaborate recovery models are as presented in Appendix B of the Supplementary Material (Appendices).

4.3. *ANOVA analysis*

This section presents a one-way ANOVA computation on the different groups of data from both experiments as considered in this paper. The essence of the one-way Anova is to investigate how the different groups of dataset from the three cutting parameters of both experiments impacts on surface roughness output. The null and alternative hypotheses were respectively defined with notations H_o *and* H_1 and further affiliated with the following arguments as presented below:

H_o :Dataset from the different cutting parameters do not significantly impact on the surface roughness output.

H_1 :Dataset from the different cutting parameters significantly impacted on the surface roughness output.

In both instances as presented in Tables 9 and 10, the calculated F values of 203.05 and 250.75 for both tables respectively are larger than the tabulated or critical F value of 3.11 at a significant level of 95%. Based on this, the null hypothesis H_o is rejected. The large disparity between and within the groups of cutting parameters, significantly impact on the surface roughness outputs. The box notch presented in Figures 11 and 12 show the median point of the cutting parameter dataset and by extension gives some clue about the divergence of the means of respective datasets of both experiments.

5. Conclusion

This paper has presented a modelling technique premised on a hybrid scheme of Gauss-Seidel difference analysis model combined with a feedback system linked to dynamic weight generation. The concept presented in this research is quite consistent with its outputs, capable of utilising small to complex datasets and gives predictive and recovery results with an error margin of approximately 0%. In addition, the proposed hybrid scheme can be applied to a variety of other predictive studies relating to materials behaviour such as cutting force predictions, acoustic emission prediction, system pressure utilisation prediction, chip size formation prediction amongst others. Beyond the world of machining, the proposed model can be adapted to daily events estimation/prediction especially when some historic data pattern or trend exists. On comparison of outputs from the proposed approach and three previously utilised techniques namely: the abductive, regression analysis and artificial neural network techniques applied to two different but similar experimental datasets, the proposed technique showed a much consistent predictive results with experimental outputs. Furthermore, the presentation of generalized algorithms adaptable to computer programmes has prompted the need to expand the design of experiment to include more levels and factors automatically ranging from 2 factors N-levels and 3-factors N-levels to some relatively high values. With this, more predictions can be carried out for both un-experimented and newly machined parameters.

Declarations

Author contribution statement

AYOMOH, M.K.O. & ABOU-EL-HOSSEIN, K.A: Conceived and designed the analysis; Analyzed and interpreted the data; Wrote the paper.

Funding statement

This research did not receive any specific grant from funding agencies in the public, commercial, or not-for-profit sectors.

Competing interest statement

The authors wish to extend their sincere gratitude to the Universities of Pretoria and Nelson Mandela Universities for resources made available to finalise this research.

Additional information

Supplementary content related to this article has been published online at https://doi.org/10.1016/j.heliyon.2021.e06338.

References

Ahmed, F., Ko, T.J., Ali, S., 2018. Analysis of the influence of input parameters of EDM on material removal rate and surface roughness for machining stainless steel 304. Int. J. Mach. Mach. Mater. 20, 78–89.

Ali, A., Hamidon, N., Zaki, N., Mokhtar, S., Azhar, A., Bahar, R., Ahmad, Z., 2018. The effect of cutting parameters on the performance of ZTA-MgO cutting tool. In: IOP Conference Series: Materials Science and Engineering. IOP Publishing, 012072.

Asiltürk, I., Neşeli, S., Ince, M.A., 2016. Optimisation of parameters affecting surface roughness of Co28Cr6Mo medical material during CNC lathe machining by using the Taguchi and RSM methods. Measurement 78, 120–128.

Ayomoh, M.K., Abou-El-Hossein, K.A., Ghobashi, S.F., 2015. Surface roughness prediction using numerical scheme and feedback control. In: Proceedings of the 10th ASME Manufacturing Science and Engineering Conference, International Manufacturing Science and Engineering Conference. American Society of Mechanical Engineers, Charlotte, North Carolina. MSEC2015-9254.

Bahgat, M.M., Shash, A.Y., Abd-Rabou, M., El-Mahallawi, I.S., 2019. Influence of process parameters in electrical discharge machining on H13 die steel. Heliyon 5 (6), e01813.

Bahgat, M.M., Shash, A.Y., Abd-Rabou, M., El-Mahallawi, I.S., 2020. Effects of process parameters on the machining process in die-sinking EDM of alloyed tool steel. In: Öchsner, A., Altenbach, H. (Eds.), Engineering Design Applications III. Advanced Structured Materials, 124. Springer, Cham, pp. 215–233.

Bajić, D., Celent, L., Jozić, S., 2012. Modeling of the influence of cutting parameters on the surface roughness, tool wear and the cutting force in face milling in off-line process control. Strojniški vestnik-Journal of Mechanical Engineering 58, 673–682.

Balaji, M., Rao, K.V., Rao, N.M., Murthy, B., 2018. Optimization of drilling parameters for drilling of TI-6Al-4V based on surface roughness, flank wear and drill vibration. Measurement 114, 332–339.

Bao, X., Ying, J., Cheng, F., Zhang, J., Luo, B., Li, L., Liu, H., 2018. Research on neural network model of surface roughness in belt sanding process for Pinus koraiensis. Measurement 115, 11–18.

Burakowski, E., Tawfik, A., Ouimette, A., Lepine, L., Novick, K., Ollinger, S., Zarzycki, C., Bonan, G., 2018. The role of surface roughness, albedo, and Bowen ratio on ecosystem energy balance in the Eastern United States. Agric. For. Meteorol. 249, 367–376.

Chen, S.-H., Ho, Y.-L., 2019. Lifespan of super-alloy Waspaloy cutting tools. Heliyon 5 (4), e01388.

Debnath, S., Reddy, M.M., Yi, Q.S., 2016. Influence of cutting fluid conditions and cutting parameters on surface roughness and tool wear in turning process using Taguchi method. Measurement 78, 111–119.

Ding, T., Zhang, S., Wang, Y., Zhu, X., 2010. Empirical models and optimal cutting parameters for cutting forces and surface roughness in hard milling of AISI H13 steel. Int. J. Adv. Manuf. Technol. 51, 45–55.

Dumitru, C., Maria, V., 2013. Advantages and disadvantages of using neural networks for predictions. Ovidius Univ. Annals, Series Econ. Sci. 13 (1), 444–449.

Feng, F., Shi, K., Xiao, S.-Z., Zhang, Y.-Y., Zhao, Z.-J., Wang, Z., Wei, J.-J., Han, Z., 2012. Fractal analysis and atomic force microscopy measurements of surface roughness for Hastelloy C276 substrates and amorphous alumina buffer layers in coated conductors. Appl. Surf. Sci. 258, 3502–3508.

Girinon, M., Karaouni, H., Masciantonio, U., Lefebvre, F., Jourden, E., Valiorgue, F., Rech, J., Feulvarch, E., 2019. Risks related to the lack of lubrication on surface integrity in drilling. Heliyon 5 (1), e01138.

Gopal, P., Prakash, K.S., 2018. Minimization of cutting force, temperature and surface roughness through GRA, TOPSIS and Taguchi techniques in end milling of Mg hybrid MMC. Measurement 116, 178–192.

Greinacher, S., Overbeck, L., Kuhnle, A., Krahe, C., Lanza, G., 2020. Multi-objective optimization of lean and resource efficient manufacturing systems. J. Inst. Eng. Prod. 14, 165–176.

Hussain, A., Lee, K., Aung, L., Abu, A., Tan, L., Kang, H., 2018. Pressure variation of developed lapping tool on surface roughness. In: IOP Conference Series: Materials Science and Engineering. IOP Publishing, 012014.

Karkalos, N., Galanis, N., Markopoulos, A., 2016. Surface roughness prediction for the milling of Ti–6Al–4V ELI alloy with the use of statistical and soft computing techniques. Measurement 90, 25–35.

Khorasani, A., Yazdi, M.R.S., 2017. Development of a dynamic surface roughness monitoring system based on artificial neural networks (ANN) in milling operation. Int. J. Adv. Manuf. Technol. 93, 141–151.

Lee, G.-J., Park, K.-H., Park, Y.-G., Park, H.-K., 2010. A quantitative AFM analysis of nano-scale surface roughness in various orthodontic brackets. Micron 41, 775–782.

Lin, G., Henriet, R., Coillet, A., Jacquot, M., Furfaro, L., Cibiel, G., Larger, L., Chembo, Y.K., 2018. Dependence of quality factor on surface roughness in crystalline whispering-gallery mode resonators. Optic Lett. 43, 495–498.

Lin, W.S., Lee, B.Y., Wu, C.L., 2001. Modelling the Surface roughness and cutting force for turning. J. Mater. Process. Technol. 108, 286–293.

Lu, X., Wang, F., Wang, X., Si, L., 2018. Modelling and optimisation of cutting parameters on surface roughness in micro-milling Inconel 718 using response surface methodology and genetic algorithm. International.

Mia, M., Razi, M.H., Ahmad, I., Mostafa, R., Rahman, S.M.S., Ahmed, D.H., Dey, P.R., Dhar, N.R., 2017. Effect of time-controlled MQL pulsing on surface roughness in hard turning by statistical analysis and artificial neural network. Int. J. Adv. Manuf. Technol. 91, 3211–3223.

Muñoz-Escalona, P., Maropoulos, P.G., 2015. A geometrical model for surface roughness prediction when face milling Al 7075-T7351 with square insert tools. J. Manuf. Syst. 36, 216–223.

Natasha, A., Ghani, J., Haron, C.C., Syarif, J., 2018. The influence of machining condition and cutting tool wear on surface roughness of AISI 4340 steel. In: IOP Conference Series: Materials Science and Engineering. IOP Publishing, 012017.

Pashmforoush, F., Bagherinia, R.D., 2018. Influence of water-based copper nanofluid on wheel loading and surface roughness during grinding of Inconel 738 superalloy. J. Clean. Prod.

Plaza, E.G., López, P.N., 2018. Analysis of cutting force signals by wavelet packet transform for surface roughness monitoring in CNC turning. Mech. Syst. Signal Process. 98, 634–651.

Rao, K.V., Murthy, B., Rao, N.M., 2014. Prediction of cutting tool wear, surface roughness and vibration of work piece in boring of AISI 316 steel with artificial neural network. Measurement 51, 63–70.

Romoli, L., 2018. Flattening of surface roughness in ultrashort pulsed laser micro-milling. Precis. Eng. 51, 331–337.

Scifo, J., Alesini, D., Anania, M., Bellaveglia, M., Bellucci, S., Biagioni, A., Bisesto, F., Cardelli, F., Chiadroni, E., Cianchi, A., 2018. Nano-machining, Surface Analysis and Emittance Measurements of a Copper Photocathode at SPARC_LAB arXiv preprint arXiv:1801.03823.

Tangjitsitcharoen, S., Thesniyom, P., Ratanakuakangwan, S., 2017. Prediction of surface Roughness in ball-end milling process by utilizing dynamic cutting force ratio. J. Intell. Manuf. 28, 13–21.

Taufik, M., Jain, P.K., 2016. A study of build edge profile for prediction of surface roughness in fused deposition modeling. J. Manuf. Sci. Eng. 138, 061002.

Ünal, E., 2018. Influence of drilling parameters on temperature and surface roughness of $AISIO_2$ steel. Mater. Testing 60, 197–201.

Vahabli, E., Rahmati, S., 2016. Application of an RBF neural network for FDM parts' surface roughness prediction for enhancing surface quality. Int. J. Precis. Eng. Manuf. 17, 1589–1603.

Weichert, D., Link, P., Stoll, A., Rueping, S., Ihlenfeldt, S., Wrobel, S., 2019. A review of machine learning for the optimization of production processes. Int. J. Adv. Manuf. Technol. 104, 1889–1902.

Xie, H., Jiang, Z., Yuen, W., 2011. Analysis of friction and surface roughness effects on edge crack evolution of thin strip during cold rolling. Tribol. Int. 44, 971–979.

Yang, F.-C., Chen, X.-P., Yue, P., 2018. Surface roughness effects on contact line motion with small capillary number. Phys. Fluids 30, 012106.

Zhang, N., Shetty, D., 2016. An effective LS-SVM-based approach for surface roughness prediction in machined surfaces. Neurocomputing 198, 35–39.

Zhao, X., Gao, Z., 2009. Surface roughness measurement using spatial-average analysis of objective speckle pattern in specular direction. Optic Laser. Eng. 47, 1307–1316.